HHS Public Access

Author manuscript

Angiogenesis. Author manuscript; available in PMC 2015 April 01.

Published in final edited form as:

Angiogenesis. 2015 April ; 18(2): 125–136. doi:10.1007/s10456-014-9450-5.

Vasculature-specific MRI reveals differential anti-angiogenic effects of a biomimetic peptide in an orthotopic breast cancer model

Eugene Kim,
Department of Biomedical Engineering, The Johns Hopkins University School of Medicine, Baltimore, MD 21205, USA

Esak Lee,
Department of Biomedical Engineering, The Johns Hopkins University School of Medicine, Baltimore, MD 21205, USA

Charlesa Plummer,
Russell H. Morgan Department of Radiology and Radiological Science, The Johns Hopkins University School of Medicine, Baltimore, MD 21205, USA

Stacy Gil,
Department of Biomedical Engineering, The Johns Hopkins University School of Medicine, Baltimore, MD 21205, USA

Aleksander S. Popel, and
Department of Biomedical Engineering, The Johns Hopkins University School of Medicine, Baltimore, MD 21205, USA

Department of Oncology, Sidney Kimmel Comprehensive Cancer Center, The Johns Hopkins University School of Medicine, 720 Rutland Ave, 217 Traylor Bldg., Baltimore, MD 21205, USA

Arvind P. Pathak
Russell H. Morgan Department of Radiology and Radiological Science, The Johns Hopkins University School of Medicine, Baltimore, MD 21205, USA

Department of Oncology, Sidney Kimmel Comprehensive Cancer Center, The Johns Hopkins University School of Medicine, 720 Rutland Ave, 217 Traylor Bldg., Baltimore, MD 21205, USA

Arvind P. Pathak: pathak@mri.jhu.edu

Abstract

Translational vasculature-specific MRI biomarkers were used to measure the effects of a novel anti-angiogenic biomimetic peptide in an orthotopic MDA-MB-231 human triple-negative breast

Correspondence to: Arvind P. Pathak, pathak@mri.jhu.edu.

Electronic supplementary material The online version of this article (doi:10.1007/s10456-014-9450-5) contains supplementary material, which is available to authorized users.

Conflict of interest ASP is a co-founder and serves as the CSO of AsclepiX Therapeutics, LLC; he also holds an equity ownership interest in this company. This arrangement has been reviewed and approved by the Johns Hopkins University in accordance with its conflict of interest policies. The other authors declare that they have no conflict of interest.

cancer model at an early growth stage. In vivo diffusion-weighted and steady-state susceptibility contrast (SSC) MRI was performed pre-treatment and 2 weeks post-treatment in tumor volume-matched treatment and control groups (n = 5/group). Treatment response was measured by changes in tumor volume; baseline transverse relaxation time (T_2); apparent diffusion coefficient (ADC); and SSC-MRI metrics of blood volume, vessel size, and vessel density. These vasculature-specific SSC-MRI biomarkers were compared to the more conventional, non-vascular biomarkers (tumor growth, ADC, and T_2) in terms of their sensitivity to anti-angiogenic treatment response. After 2 weeks of peptide treatment, tumor growth inhibition was evident but not yet significant, and the changes in ADC or T_2 were not significantly different between treated and control groups. In contrast, the vascular MRI biomarkers revealed a significant anti-angiogenic response to the peptide after 2 weeks—blood volume and vessel size decreased, and vessel density increased in treated tumors; the opposite was seen in control tumors. The MRI results were validated with histology—H&E staining showed no difference in tumor viability between groups, while peptide-treated tumors exhibited decreased vascularity. These results indicate that translational SSC-MRI biomarkers are able to detect the differential effects of anti-angiogenic therapy on the tumor vasculature before significant tumor growth inhibition or changes in tumor viability.

Keywords

Angiogenesis; Biomarker; Breast cancer; Imaging; Peptide therapy; Susceptibility contrast MRI

Introduction

Angiogenesis is one of the hallmarks of cancer and is essential for the progression and metastasis of most solid tumors [1]. Although several anti-angiogenic drugs have been approved by the US Food and Drug Administration (FDA) to treat certain cancers, none are currently approved for treating breast cancer [2]. Therefore, there is an exigent need for novel targeted therapies, particularly for triple-negative breast cancer (TNBC), an aggressive subtype of breast cancer with poor prognosis that is unresponsive to current receptor-targeted therapies [3]. Since TNBC tends to be highly vascularized and expresses elevated levels of vascular endothelial growth factor (VEGF) [4, 5], anti-angiogenic therapies have the potential to improve TNBC patient outcomes.

Recently, peptides have emerged as promising new therapeutic agents because they exhibit advantages over large protein or small-molecule therapeutics, such as low-molecular weights below the immunogenic threshold; superior synthetic fidelity since peptide synthesis is based on amino acids, which are standardized building blocks; and high diversity since single amino acid substitutions can be made to engineer more specific interaction of the peptide with target molecules. We have identified more than 100 anti-angiogenic peptides using a bioinformatics-based methodology [6]. Among them, peptides derived from collagen type IV potently inhibited angiogenesis in vivo and in vitro [7, 8]. In this study, we evaluated the in vivo efficacy of SP2024, a new variant of these biomimetic peptides that has been shown to interfere with integrin β1 interactions as well as vascular endothelial growth factor receptor 2 (VEGFR2) signaling pathways in endothelial cells [9].

In addition to the need for improved anti-angiogenic therapies, there is a need for translational in vivo biomarkers to assess and optimize the efficacy of such therapies [10]. Magnetic resonance imaging (MRI) has demonstrated the potential to provide such translational biomarkers of angiogenesis [11]. For example, steady-state susceptibility contrast (SSC) MRI has been used to measure blood volume, vessel size, and vessel density [12]. It is an established preclinical technique wherein an intravascular (super) paramagnetic contrast agent (e.g., ultra-small superparamagnetic iron oxide nanoparticles) is administered to increase the magnetic susceptibility gradients between the intra- and extravascular spaces. This produces a measurable increase in the transverse relaxation rates of spin echo and gradient echo MRI signals ($R_2 = 1/T_2$ and $R_2^*=1/T_2^*$, respectively) [13], which can then be exploited to compute in vivo biomarkers of vascular morphology [14–16]. This method has been used to monitor tumor response to anti-angiogenic treatments in various preclinical cancer models [17–23]. The potential for clinical translation of SSC-MRI has been enhanced by the availability of ferumoxytol (Feraheme®, AMAG Pharmaceuticals, Inc., Lexington, MA), an FDA-approved drug that can also be used as a superparamagnetic MRI contrast agent. Several Phase 1 and Phase 2 clinical trials have been conducted or are currently underway to evaluate the safety and efficacy of ferumoxytol as a clinical MRI contrast agent [24, 25].

The current study had two primary aims. The first aim was to use SSC-MRI to characterize the effects of SP2024 peptide treatment on tumor blood volume, vessel size, and vessel density in early-stage orthotopic human TNBC xenografts in mice. In addition, diffusion-weighted imaging (DWI) was used to measure the in vivo apparent diffusion coefficients (ADC), a promising biomarker of treatment-induced changes in tumor cellularity [26]. However, ADC is not directly related to tumor vascularity, and changes in tumor cellularity may occur later than changes in the tumor vasculature following anti-angiogenic therapy. The second aim of this study was to test the hypothesis that the vasculature-specific SSC-MRI biomarkers are more sensitive than tumor size or ADC to the effects of our anti-angiogenic peptide.

Materials and methods

Cell culture and inoculation

MDA-MB-231 human breast cancer cells were grown in RPMI-1640 cell culture medium supplemented with 10 % fetal bovine serum and 1 % penicillin–streptomycin (Sigma-Aldrich, St. Louis, MO). Three million MDA-MB-231 cells in 50 μL of Hank's balanced salt solution (Sigma-Aldrich) were orthotopically inoculated into the lower right thoracic mammary fat pad of 10 female athymic NCr-*nu/nu* mice anesthetized with Ketamine (80 mg/kg)/Xylazine (5 mg/kg) administered i.p. All animal studies were performed in accordance with the institutional Animal Care and Use Committee guidelines.

In vivo MRI acquisition

When tumor xenografts had grown to approximately 70 mm^3, they were imaged in vivo on a Bruker Biospin (Billerica, MA) 9.4T small animal MRI system using an 18-mm-diameter radiofrequency transceiver surface coil using the following sequences: (1) two-dimensional

(2D) diffusion-weighted imaging (DWI), echo time (TE) = 26.6 ms, repetition time (TR) = 1,000 ms; one non-diffusion-weighted and three diffusion-weighted images with *b* value = 327 s/mm^2 and diffusion-sensitizing gradient orientations along the *x*-, *y*-, and *z*-axes were acquired. (2) 2D multiple gradient echo (MGE), TE = 5 ms, six echoes with 5 ms echo spacing, TR = 800 ms. (3) 2D multiple spin echo (MSE), TE = 10 ms, eight echoes with 10 ms echo spacing, TR = 1500 ms. MGE and MSE images were acquired before and 5 min after i.v. injection of ferumoxytol at a dose of 5 mg Fe/kg. For all imaging sequences, in-plane resolution = 125 μm, slice thickness = 1 mm, and the number of slices varied to cover the entire extent of each tumor. The imaging time for each mouse was approximately 1 h. Further details of the imaging protocol and sequences can be found in [12].

Peptide synthesis and treatment

The SP2024 peptide was produced by a commercial manufacturer (New England Peptide, Gardner, MA) using a solid-phase synthesis technique. High-performance liquid chromatography and mass spectrometry analyses of the peptide were provided by the manufacturer to demonstrate greater than 95 % purity. For the preparation of peptide stock solutions, DMSO (Sigma-Aldrich, St. Louis, MO) was used as a solvent at a concentration of 5 % (vol/vol) in PBS. The peptide stock was stored at −80 °C and thawed at room temperature just before use. Prior to imaging, mice were randomized into two groups of five animals each. Starting on the day of the pre-treatment scans (day 0), one group received daily i.p. injections of 100 μL of SP2024 solution at a dose of 10 mg/kg, while the other group received daily i.p. injections of 100 μL of 5 % DMSO in PBS to control for solvent effects. Tumor volumes (*V*) were measured daily using the formula: $V = 0.52ab^2$, where *a* is the long axis and *b* the short axis of the tumor, measured by a caliper.

After 14 days of treatment, tumors were imaged again (day 14) using the same in vivo MRI protocol as for day 0. Fourteen days were chosen as a suitable early growth stage time point based on the tumor volume (~70 mm^3). Typical imaging studies using xenografts derived from the MDA-MB-231 cell line employ tumors in the 100–1,000 mm^3 volume range [27, 28]. In this study, we used early-stage tumors to avoid confounding effects from necrosis and possible anti-angiogenic resistance.

Histology

Following the in vivo MRI experiments, mice were sacrificed by cervical dislocation. The tumors were immediately excised and immersion-fixed in freshly prepared 2 % formaldehyde at 4 °C for 48 h. The samples were then transferred to 30 % sucrose + 0.02 % sodium azide in PBS and stored at 4 °C for 2 weeks. The fixed, cryoprotected tumor samples were embedded in Tissue-Tek Optimum Cutting Temperature (O.C.T.) Compound (Sakura Finetek USA, Inc., Torrance, CA) and frozen in liquid nitrogen. Serial 12 μm-thick sections were cut at −20 °C and mounted for H&E and immunofluorescent staining of laminin (an endothelial basement membrane protein), VEGF165, and phosphorylated Met receptor tyrosine kinase (p-Met; Online Resource 1). Met is activated by phosphorylation via binding of its natural ligand, hepatocyte growth factor (HGF). Met in turn activates multiple signal transducers such as phospholipase C-γ (PLC-γ), mitogen-activated protein kinase (MAPK), phosphatidylinositol 3-kinase (PI3K), and focal adhesion kinase (FAK) [29]. These

downstream Met signaling pathways are important for angiogenesis and cell migration, proliferation, and survival.

Tumor viability quantification—A Nikon DXM1200 microscope was used to acquire color images of H&E-stained breast tumor sections at 2× magnification. Several images were taken to cover each whole section. ImageJ (National Institutes of Health, Bethesda, MD) was used to apply background subtraction and to stitch together the different fields taken for each tumor section to create an image montage of the whole section. Color H&E images were converted to grayscale images. The darker regions, indicative of abundant hematoxylin staining, were considered viable tumor regions; lighter regions stained only with eosin were considered non-viable or necrotic. The grayscale images were binarized using the default ImageJ automatic threshold algorithm to quantify the viable tumor fraction from each tumor section.

Quantitative immunofluorescence microscopy—Laminin fluorescence images were obtained at 10× magnification using a Nikon Eclipse E400 microscope (Nikon Instruments Inc., Melville, NY). Twenty-nine and 24 random fields were acquired from five control and four treated tumors, respectively. Using ImageJ, a median filter (two-pixel radius) and background subtraction (50-pixel radius rolling ball) were applied before manually thresholding the images and measuring the laminin-positive area fractions. The average laminin-positive area fraction was calculated for each tumor.

VEGF165 and p-Met fluorescence images were obtained at 10× magnification using an LSM-510 confocal microscope (Carl Zeiss Microscopy GmbH, Jena, Germany). Twenty-four random fields were acquired for each marker from three control tumors and three treated tumors. VEGF165 and p-Met-positive signals were binarized using the default ImageJ automatic threshold algorithm, and the positive area fractions were measured. The average VEGF165- and p-Met-positive area fractions were calculated for each tumor.

Measurement of ferumoxytol-induced Δχ

The difference in magnetic susceptibility induced by ferumoxytol ($\Delta\chi_c$) was measured using the same MRI scanner and radiofrequency coil used for the in vivo experiments. A tube filled with saline was placed in the coil perpendicular to the main magnetic field (B_0). The resonant frequency was measured inside a 4-mm isotropic voxel placed in the center of the tube. This was repeated for a tube filled with ferumoxytol diluted with saline to the concentration used for the in vivo scans. $\Delta\chi_c$ was calculated using the equation for the Lorentz-corrected frequency shift inside a cylindrical, magnetized object oriented perpendicular to B_0:

$$\Delta\chi_c = -\frac{3\left(\omega_{\text{post-contrast}} - \omega_{\text{pre-contrast}}\right)}{2\pi\gamma B_0} \quad (1)$$

In vivo MRI processing

Tumor masks were manually drawn on pre-contrast T_2-weighted SE images using the Analysis of Functional NeuroImages (AFNI) software [30] and used to exclude voxels

containing non-tumor tissue from all subsequent image analyses. ADC, R_2^*, and R_2 maps were computed on a voxel-wise basis using methods described by us in [12]. Briefly, ADC maps were calculated from the DWI images using DTI Studio (H Jiang and S Mori, Department of Radiology, Johns Hopkins University, Baltimore, MD). R_2^* and R_2 maps were generated in AFNI by fitting the MGE and MSE signal intensity time courses to a mono-exponential decay model with a constant noise term. The *F*-statistic was used to discard any voxels for which the full exponential model did not fit the data significantly better than a simple constant model. The differences between post- and pre-contrast $R_2^{(*)}$ were computed, and voxels with negative $\Delta R_2^{(*)}$ were excluded from further analysis. Voxel-wise maps of the following in vivo MRI biomarkers were also computed

$$\mathrm{FBV}=\frac{3}{4\pi}\frac{\Delta R_2^*}{\gamma\Delta\chi_c B_0} \quad (2)$$

$$R\equiv\frac{\Delta R_2^*}{\Delta R_2} \quad (3)$$

$$\mathrm{VSI}=0.425\left(\frac{\mathrm{ADC}}{\gamma\Delta\chi_c B_0}\right)^{1/2}R^{3/2} \quad (4)$$

$$Q\equiv\frac{\Delta R_2}{(\Delta R_2^*)^{2/3}} \quad (5)$$

$$N=\frac{Q^3}{\mathrm{ADC}} \quad (6)$$

where γ is the gyromagnetic ratio of the ^{1}H nucleus, and B_0 is the main magnetic field strength. FBV is fractional blood volume [16], *R* is a measure of vessel radius [14], VSI is the vessel size index [16], and *Q* and *N* are measures of vessel density (i.e., number of vessel branches per unit area) [15]. ΔR_2 was considered as a biomarker of microvascular blood volume [31]. ADC and pre-contrast T_2 were considered as biomarkers of tumor cellularity [26, 32].

Statistical analysis

The two-tailed Mann–Whitney *U* test ($\alpha = 0.05$) was performed to determine (1) whether there was a significant difference in tumor volume and growth between control and treatment groups; (2) whether the change in the tumor-wise median of each MRI parameter from day 0 to day 14 was significantly different between control and treatment groups; and (3) whether histologically measured viable tumor fraction and laminin area fraction were significantly different between control and treatment groups.

A mutual information metric was used to quantify the utility of each measured parameter (tumor volume, pre-contrast T_2, ADC, FBV, ΔR_2, VSI, *R*, *Q*, and *N*) as a biomarker of

SP2024 treatment response. First, the percent change in the median value of each parameter (ΔX) for each tumor was binarized by applying a threshold t:

$$\Delta X_t = \begin{cases} 1, & \Delta X > t \\ 0, & \Delta X \leq t \end{cases} \quad (7)$$

Then, the mutual information $I(\Delta X_t, G)$ between these binary parameter changes ΔX_t and group membership ($G \in$ [control, treatment]) was calculated as:

$$I(\Delta X_t, G) = H(G) - H(G|\Delta X_t) \quad (8)$$

The marginal entropy $H(G) = 1$ because the control and treatment groups were of equal size. The conditional entropy $H(G|\Delta X_t)$ was computed using the following equation:

$$H(G|\Delta X_t) = -\sum_{x \in \Delta X_t} p(x) \sum_{g \in G} p(g|x) \log_2 p(g|x) \quad (9)$$

where $p(x)$ is the probability that $\Delta X_t = x$ and $p(g|x)$ is the conditional probability that $G = g$ given $\Delta X_t = x$. For each parameter, the maximum mutual information as a function of the threshold (I_{max}) as well as the mutual information given a threshold of zero ($I_{t=0}$) were calculated.

Results

Ferumoxytol-induced Δχ

The resonance frequency was 3.91 Hz in saline and −74.34 Hz in the ferumoxytol solution with an iron concentration equivalent to the in vivo dose of 5 mg/kg. This corresponded to a $\Delta\chi_c$ of 0.09 ppm (cgs units) as calculated by Eq. (1).

Effect of SP2024 on tumor growth

There was no difference in tumor volume at day 0 between treatment (68.2 ± 8.02 mm^3, median ± median absolute deviation) and control (67.8 ± 11.0 mm^3) groups. While the treated tumors grew more slowly compared to the control tumors (Fig. 1a), the tumor sizes at day 14 (98.6 ± 17.9 mm^3 for treated and 185.0 ± 98.8 mm^3 for control) were still not significantly different between the two groups ($p = 0.1$). There was also no significant difference in the change in tumor volume from day 0 to day 14 ($p = 0.06$; Table 1; Fig. 1b).

Effect of SP2024 on in vivo MRI biomarkers

Figure 2 shows MRI parametric maps from a representative control tumor at day 0 and day 14. The first row shows pre-contrast spin echo (SE, TE = 40 ms) and gradient echo (GE, TE = 5 ms) images. Below, the parametric maps are overlaid on their respective SE images. Figure 3 shows corresponding images for a representative treated tumor. Voxels in the maps that had negative $\Delta R_2^{(*)}$ or that did not meet the F-statistic criterion were not displayed.

The median pre-contrast T_2 increased from day 0 to day 14 in all control tumors and all but one treated tumor; there was no significant difference in the change in median T_2 between groups (Fig. 4a). There was also no significant difference in the change in median ADC between control and treatment groups, with positive and negative changes observed in both groups (Fig. 4b). With the exception of ΔR_2, all vascular biomarkers exhibited significantly different changes between control and treatment groups (Fig. 4c–h). In general, median FBV, *R*, and VSI increased while ΔR_2, *Q*, and *N* decreased from day 0 to day 14 in the control tumors. In contrast, median FBV, *R*, and VSI decreased while ΔR_2, *Q*, and *N* increased in the treated tumors.

Figure 5 shows a radar plot summarizing the percent change in the median value of each non-vascular and vascular biomarker for the SP2024-treated and control groups. Table 1 lists the absolute and percent changes in median biomarker values for each group and the *p* values from the two-tailed Mann–Whitney *U* tests to compare the changes between control and treatment groups.

The ability of each biomarker to predict whether a mouse received treatment was measured by the mutual information (*I*) between group membership and the percent change in that biomarker. $I = 1$ indicates that knowing the percent change in the median value of a particular biomarker in a tumor from day 0 to day 14 removes all uncertainty of that tumor's group membership, i.e., there is no overlap between control and treatment groups. Comparing values of I_{max} suggests that all of the vascular biomarkers were as good as or better than the non-vascular biomarkers at predicting group membership (Table 2). In fact, there was no overlap between the control and treated tumors in the change in median FBV, *R*, VSI, *N*, or *Q* ($I_{max} = 1$). The $I_{t=0}$ values indicate that if it were only known whether a biomarker increased or decreased, all of the vascular biomarkers would be better predictors of group membership than any of the non-vascular biomarkers.

Histology

Figure 6 shows raw images of H&E sections from representative control and treated tumors (Fig. 6a, b), and the corresponding binarized images in which black areas represent viable tumor (Fig. 6c, d). There was no significant difference in the viable tumor fraction calculated from H&E images between control (43.5 ± 4.4 %, median ± median absolute deviation) and treated tumors (46.6 ± 0.5 %; Fig. 6e). This is consistent with the ADC and T_2 measurements, which did not detect a cellular response to treatment. In contrast, significantly less laminin staining was observed in treated tumors (0.018 ± 0.003 fractional area) than in control tumors (0.062 ± 0.002; Fig. 7a–c), which is consistent with the SSC-MRI data and indicative of the anti-angiogenic activity of the SP2024 peptide. Concordantly, VEGF expression was lower in the treated tumors (0.032 ± 0.007) than in control tumors (0.093 ± 0.013; Fig. 7d–e). Treated tumors also had lower levels of p-Met (0.067 ± 0.007) compared to control tumors (0.323 ± 0.088; Fig. 7f–g).

Discussion

Treatment with the SP2024 peptide induced strong anti-angiogenic effects in early-stage MDA-MB-231 human breast cancer xenografts, as demonstrated by the significant changes

in SSC-MRI biomarkers of blood volume, vessel size, and vessel density. In contrast, changes in ADC and T_2 were not significant between the treatment and control groups. While SP2024 treatment did reduce tumor growth rates, this reduction in tumor growth was not significant over the two-week treatment period. Collectively, these results indicate that the vasculature-specific MRI biomarkers were more sensitive to the effects of SP2024 than tumor volume, ADC, or T_2. This sensitivity was quantified in terms of the mutual information metric (Table 2) and illustrated by the radar plot in Fig. 5.

While anti-angiogenic therapy also has anti-tumor effects, typically vascular changes have been shown to precede tumor growth inhibition [33–35]. Changes in ADC have also been shown to be predictive of response to anti-angiogenic therapy [36] and to precede changes in tumor size [35], but in this study, control and treated tumors were not distinguishable from changes in ADC. A recent study showed that SP2024 induced apoptosis in MDA-MB-231 xenografts as measured by cleaved caspase-3 activity [37]. Therefore, decreased cell density due to apoptosis may have contributed to the increased median ADC in three of the five treated tumors. Interestingly, median ADC increased in three of the five control tumors as well, possibly due to increased edema or necrosis.

Analogously, it is possible that tumor vasculature may naturally evolve in a way that can obscure anti-angiogenic treatment effects. For example, we previously observed lower fractional blood volumes in MDA-MB-231 tumors at post-inoculation week (PIW) 5 compared to tumors at PIW 3 [12]. The presence of necrosis in the larger tumors suggests that the decreased fractional blood volume was primarily caused by tumor growth outstripping the available blood supply. Since anti-angiogenic therapy is expected to decrease tumor blood volume, treatment for this study was initiated when the tumors were smaller than the PIW 3 tumors from our previous study to ensure that the blood volume did not also decrease in the control tumors during the two-week treatment period.

The increased FBV and VSI in control tumors seen here are consistent with the elevated blood volume and dilated vessels that result from VEGF-driven pathological angiogenesis in tumors [38]. Treated tumors demonstrated a direct reversal of this vascular phenotype, with decreased FBV and VSI after SP2024 treatment. The SP2024-induced decrease in blood volume was corroborated by the significantly reduced laminin staining in treated tumors compared to control tumors. However, it should be borne in mind that laminin, while a component of the vascular basement membrane, does not label the intraluminal space. This makes direct quantification of blood volume, vessel radii, and density by stereologic methods challenging [39]. Therefore, an alternative validation technique for preclinical studies would be to perfuse the animal with a vascular filling agent such as Microfil® (FlowTech Inc., Carver, MA) and acquire high-resolution micro-CT images of the vasculature [12].

As demonstrated by the mutual information analysis, one could not distinguish between control and treatment groups based on changes in median ΔR_2 in contrast to the other SSC-MRI biomarkers (Table 2). This may be explained by the opposing effects that blood volume and vessel radius have on ΔR_2, which increases with increasing blood volume but decreases with increasing vessel radius (after peaking at a radius that typically corresponds

to capillary-sized vessels) [31]. In general, ΔR_2 decreased in control tumors, which was consistent with a decrease in microvascular volume fraction that was likely due to vessel dilation. The one control tumor in which median ΔR_2 increased also exhibited the largest increase in median FBV. This suggests that the decrease in ΔR_2 caused by decreased microvascular volume in control tumors may be offset to some degree by an increase in total blood volume. The opposite trend was seen in the treated tumors—VSI and *R* decreased in all treated tumors and ΔR_2 increased in three. This suggests that SP2024 therapy decreased average vessel caliber and increased the relative number of small vessels to which ΔR_2 is most sensitive, thereby increasing ΔR_2. Collectively, these observations suggest that SP2024 preferentially prunes larger tumor blood vessels. However, the median ΔR_2 decreased in two treated tumors, which may be attributed to the countervailing effect of decreased total blood volume, which was observed in all treated tumors. Overall, our results indicate that knowing both ΔR_2^* and ΔR_2 is more informative for resolving the differential effects of anti-angiogenic therapy than knowing either parameter alone.

The reduction in vessel caliber observed in the SP2024-treated tumors is a characteristic response to anti-angiogenic treatment that has been reported in many preclinical and clinical studies, which are summarized in a recent review by Emblem et al. [40]. While anti-angiogenic agents are known to inhibit the sprouting of new vessels, they can also affect a wider population of tumor vessels resulting in complex vascular remodeling [23]. For example, although it might be expected that anti-angiogenic therapy would decrease vessel density, the SSC-MRI-measured vessel density increased in the SP2024-treated tumors and decreased in the control tumors. The concomitant decrease in vessel caliber and increase in vessel density found here is suggestive of vascular normalization [41]. Moreover, the absence of a cellular response as assessed by histology and DW-MRI despite a significant decrease in fractional blood volume in the treated tumors indicates that SP2024-induced vascular remodeling may have resulted in improved tumor perfusion, although validation of this hypothesis was outside the scope of this study.

It must be mentioned that the microvessel density biomarker, *N*, is not an independent metric but a function of FBV and VSI—Eq. (6) is derived directly by substituting Eqs. (2) and (4) into $N = \mathrm{FBV}/(2\pi \mathrm{VSI}^2)$ [15]. Therefore, any measurement errors or noise in the assessment of FBV and VSI will propagate to calculations of *N*. Even if FBV and VSI correctly reflect the decreased blood volume and vessel caliber in treated tumors, errors in the magnitudes of these changes could have caused a spurious increase in *N*.

However, we have previously shown using high-resolution μCT that vessel density decreases in MDA-MB-231 tumors with tumor progression and that *N* and *Q* correlated with μCT-measured vessel density [12]. It is therefore possible that SP2024 treatment remodels the vascular phenotype in a way that results in an increase in microvessel density assessed by MRI. And as discussed in the review by Hlatky et al. [42], microvessel density is not a simple indicator of angiogenic activity and can fluctuate during the course of anti-angiogenic therapy. This underscores the need for more sensitive and noninvasive clinical biomarkers capable of repeated measurements for longitudinal patient monitoring. Such a biomarker would enable more flexible and adaptive clinical trial design and treatment regimens. In this regard, MRI is superior to conventional biopsy and histological evaluations

of anti-angiogenic treatment efficacy, but its repeatability is limited by cost, MRI scanner availability, and for contrast-enhanced methods, the biological and plasma half-lives of the contrast agent.

Immunofluorescence microscopy data showed that SP2024-treated tumors exhibited reduced VEGF165 expression and Met receptor activation, which suggests that the peptide may inhibit angiogenesis via multiple pathways. For example, SP2024 has been shown to inhibit integrin β1 interactions and phosphorylation of VEGFR2 as well as downstream signal transducers PLC-γ and FAK in endothelial cells [37]. Met has several of the same downstream targets as VEGFR2, including PLC-γ, MAPK, FAK, and PI3K [43]. Our data are also consistent with observations by Munshi et al. [44] showing that treatment with a selective Met inhibitor significantly inhibited in vitro proliferation and in vivo tumor xenograft growth in several human cancer cell lines including MDA-MB-231. Studies have also shown that Met signaling may be an alternative pathway via which tumors can evade anti-VEGF therapy [45–47]. Therefore, agents such as SP2024 that target multiple pathways involved in angiogenesis could circumvent the problems of acquired anti-angiogenic resistance and increased invasiveness that can result from prolonged inhibition of the VEGF pathway [48]. Future work includes assessing the effects of SP2024 on breast cancer metastasis and its robustness against anti-angiogenic resistance.

In conclusion, we have demonstrated that SP2024 has a potent anti-angiogenic effect in an orthotopic triple-negative breast cancer model. Furthermore, SSC-MRI was highly sensitive to treatment-induced vascular remodeling and could provide much-needed biomarkers of treatment response in future clinical trials of anti-angiogenic agents.

Acknowledgments

The authors would like to thank Dr. Yoshinori Kato for graciously lending his deft touch for tail vein cannulations. Research was funded by Komen Foundation Grant KG09640 (APP) and NIH Grant R01 CA138264 (ASP).

References

1. Hanahan D, Weinberg RA. Hallmarks of cancer: the next generation. Cell. 2011; 144(5):646–674. [PubMed: 21376230]
2. Mackey JR, Kerbel RS, Gelmon KA, McLeod DM, Chia SK, Rayson D, Verma S, Collins LL, Paterson AH, Robidoux A, Pritchard KI. Controlling angiogenesis in breast cancer: a systematic review of anti-angiogenic trials. Cancer Treat Rev. 2012; 38(6):673–688. [PubMed: 22365657]
3. Greenberg S, Rugo HS. Triple-negative breast cancer: role of antiangiogenic agents. Cancer J. 2010; 16(1):33–38. [PubMed: 20164688]
4. Linderholm BK, Hellborg H, Johansson U, Elmberger G, Skoog L, Lehtio J, Lewensohn R. Significantly higher levels of vascular endothelial growth factor (VEGF) and shorter survival times for patients with primary operable triple-negative breast cancer. Ann Oncol. 2009; 20(10):1639–1646. [PubMed: 19549711]
5. Nalwoga H, Arnes JB, Stefansson IM, Wabinga H, Foulkes WD, Akslen LA. Vascular proliferation is increased in basallike breast cancer. Breast Cancer Res Treat. 2011; 130(3):1063–1071. [PubMed: 21874512]
6. Karagiannis ED, Popel AS. A systematic methodology for proteome-wide identification of peptides inhibiting the proliferation and migration of endothelial cells. Proc Natl Acad Sci USA. 2008; 105(37):13775–13780. [PubMed: 18780781]

7. Rosca EV, Koskimaki JE, Pandey NB, Tamiz AP, Popel AS. Structure-activity relationship study of collagen-derived anti-angiogenic biomimetic peptides. Chem Biol Drug Des. 2012; 80(1):27–37. [PubMed: 22405100]
8. Rosca EV, Lal B, Koskimaki JE, Popel AS, Laterra J. Collagen IV and CXC chemokine-derived antiangiogenic peptides suppress glioma xenograft growth. Anticancer Drugs. 2012; 23(7):706–712. [PubMed: 22495619]
9. Koskimaki JE, Lee E, Chen W, Rivera CG, Rosca EV, Pandey NB, Popel AS. Synergy between a collagen IV mimetic peptide and a somatotropin-domain derived peptide as angiogenesis and lymphangiogenesis inhibitors. Angiogenesis. 2013; 16(1):159–170. [PubMed: 23053781]
10. Sessa C, Guibal A, Del Conte G, Ruegg C. Biomarkers of angiogenesis for the development of antiangiogenic therapies in oncology: tools or decorations? Nat Clin Pract Oncol. 2008; 5(7):378–391. [PubMed: 18560389]
11. Pathak AP, Hochfeld WE, Goodman SL, Pepper MS. Circulating and imaging markers for angiogenesis. Angiogenesis. 2008; 11(4):321–335. [PubMed: 18925424]
12. Kim E, Cebulla J, Ward BD, Rhie K, Zhang J, Pathak AP. Assessing breast cancer angiogenesis in vivo: which susceptibility contrast MRI biomarkers are relevant? Magn Reson Med. 2013; 70(4): 1106–1116. [PubMed: 23225578]
13. Kennan RP, Zhong J, Gore JC. Intravascular susceptibility contrast mechanisms in tissues. Magn Reson Med. 1994; 31(1):9–21. [PubMed: 8121277]
14. Dennie J, Mandeville JB, Boxerman JL, Packard SD, Rosen BR, Weisskoff RM. NMR imaging of changes in vascular morphology due to tumor angiogenesis. Magn Reson Med. 1998; 40(6):793–799. [PubMed: 9840821]
15. Jensen JH, Chandra R. MR imaging of microvasculature. Magn Reson Med. 2000; 44(2):224–230. [PubMed: 10918321]
16. Tropres I, Grimault S, Vaeth A, Grillon E, Julien C, Payen JF, Lamalle L, Decorps M. Vessel size imaging. Magn Reson Med. 2001; 45(3):397–408. [PubMed: 11241696]
17. Bauerle T, Merz M, Komljenovic D, Zwick S, Semmler W. Drug-induced vessel remodeling in bone metastases as assessed by dynamic contrast enhanced magnetic resonance imaging and vessel size imaging: a longitudinal in vivo study. Clin Cancer Res. 2010; 16(12):3215–3225. [PubMed: 20530698]
18. Farrar CT, Kamoun WS, Ley CD, Kim YR, Catana C, Kwon SJ, Rosen BR, Jain RK, Sorensen AG. Sensitivity of MRI tumor biomarkers to VEGFR inhibitor therapy in an orthotopic mouse glioma model. PLoS One. 2011; 6(3):e17228. [PubMed: 21390238]
19. Nielsen T, Bentzen L, Pedersen M, Tramm T, Rijken PF, Bussink J, Horsman MR, Ostergaard L. Combretastatin A-4 phosphate affects tumor vessel volume and size distribution as assessed using MRI-based vessel size imaging. Clin Cancer Res. 2012; 18(23):6469–6477. [PubMed: 23071260]
20. Ullrich RT, Jikeli JF, Diedenhofen M, Bohm-Sturm P, Unruh M, Vollmar S, Hoehn M. In-vivo visualization of tumor microvessel density and response to anti-angiogenic treatment by high resolution MRI in mice. PLoS One. 2011; 6(5):e19592. [PubMed: 21573168]
21. Ungersma SE, Pacheco G, Ho C, Yee SF, Ross J, van Bruggen N, Peale FV Jr, Ross S, Carano RA. Vessel imaging with viable tumor analysis for quantification of tumor angiogenesis. Magn Reson Med. 2010; 63(6):1637–1647. [PubMed: 20512867]
22. Walker-Samuel S, Boult JK, McPhail LD, Box G, Eccles SA, Robinson SP. Non-invasive in vivo imaging of vessel calibre in orthotopic prostate tumour xenografts. Int J Cancer. 2011; 130(6): 1284–1293. [PubMed: 21469141]
23. Zwick S, Strecker R, Kiselev V, Gall P, Huppert J, Palmowski M, Lederle W, Woenne EC, Hengerer A, Taupitz M, Semmler W, Kiessling F. Assessment of vascular remodeling under antiangiogenic therapy using DCE-MRI and vessel size imaging. J Magn Reson Imaging: JMRI. 2009; 29(5):1125–1133.
24. Fredrickson J, Serkova N, Carano RA, Wyatt S, Pirzkall A, Weekes C, Silverman J, Rosen L, de Crespigny A. Clinical translation of VSI using ferumoxytol: feasibility in a phase I oncology clinical trial population. Proc Intl Soc Mag Reson Med. 2012; 20:1987.
25. Stabi KL, Bendz LM. Ferumoxytol use as an intravenous contrast agent for magnetic resonance angiography. Ann Pharmacother. 2011; 45(12):1571–1575. [PubMed: 22045905]

26. Thoeny HC, Ross BD. Predicting and monitoring cancer treatment response with diffusion-weighted MRI. J Magn Reson Imaging. 2010; 32(1):2–16. [PubMed: 20575076]
27. Cyran CC, Sennino B, Fu Y, Rogut V, Shames DM, Chaopathomkul B, Wendland MF, McDonald DM, Brasch RC, Raatschen HJ. Permeability to macromolecular contrast media quantified by dynamic MRI correlates with tumor tissue assays of vascular endothelial growth factor (VEGF). Eur J Radiol. 2012; 81(5):891–896. [PubMed: 21889860]
28. Zhang X, Pagel MD, Baker AF, Gillies RJ. Reproducibility of magnetic resonance perfusion imaging. PLoS One. 2014; 9(2):e89797. [PubMed: 24587040]
29. Christensen JG, Burrows J, Salgia R. c-Met as a target for human cancer and characterization of inhibitors for therapeutic intervention. Cancer Lett. 2005; 225(1):1–26. [PubMed: 15922853]
30. Cox RW. AFNI: software for analysis and visualization of functional magnetic resonance neuroimages. Comput Biomed Res Int J. 1996; 29(3):162–173.
31. Boxerman JL, Hamberg LM, Rosen BR, Weisskoff RM. MR contrast due to intravascular magnetic susceptibility perturbations. Magn Reson Med. 1995; 34(4):555–566. [PubMed: 8524024]
32. Jakobsen I, Lyng H, Kaalhus O, Rofstad EK. MRI of human tumor xenografts in vivo: proton relaxation times and extracellular tumor volume. Magn Reson Imaging. 1995; 13(5):693–700. [PubMed: 8569443]
33. Hoff BA, Bhojani MS, Rudge J, Chenevert TL, Meyer CR, Galban S, Johnson TD, Leopold JS, Rehemtulla A, Ross BD, Galban CJ. DCE and DW-MRI monitoring of vascular disruption following VEGF-Trap treatment of a rat glioma model. NMR Biomed. 2012; 25(7):935–942. [PubMed: 22190279]
34. Lindner DJ, Borden EC. Effects of tamoxifen and interferon-beta or the combination on tumor-induced angiogenesis. Int J Cancer. 1997; 71(3):456–461. [PubMed: 9139884]
35. Sahani DV, Jiang T, Hayano K, Duda DG, Catalano OA, Ancukiewicz M, Jain RK, Zhu AX. Magnetic resonance imaging biomarkers in hepatocellular carcinoma: association with response and circulating biomarkers after sunitinib therapy. J Hematol Oncol. 2013; 6:51. [PubMed: 23842041]
36. Nowosielski M, Recheis W, Goebel G, Guler O, Tinkhauser G, Kostron H, Schocke M, Gotwald T, Stockhammer G, Hutterer M. ADC histograms predict response to anti-angiogenic therapy in patients with recurrent high-grade glioma. Neuroradiology. 2010; 53(4):291–302. [PubMed: 21125399]
37. Rosca, EV.; Penet, MF.; Koskimaki, JE.; Pandey, NB.; M, BZ.; Popel, AS. Proceedings of the 102nd Annual Meeting of the American Association for Cancer Research. Vol. 8. Orlando, FL: 2011. Biomimetic anti-angiogenic peptide as therapeutic agent for breast cancer [abstract].
38. Carmeliet P. VEGF as a key mediator of angiogenesis in cancer. Oncology. 2005; 69(Suppl 3):4–10. [PubMed: 16301830]
39. Pathak AP, Schmainda KM, Ward BD, Linderman JR, Rebro KJ, Greene AS. MR-derived cerebral blood volume maps: issues regarding histological validation and assessment of tumor angiogenesis. Magn Reson Med. 2001; 46(4):735–747. [PubMed: 11590650]
40. Emblem KE, Farrar CT, Gerstner ER, Batchelor TT, Borra RJ, Rosen BR, Sorensen AG, Jain RK. Vessel calibre-a potential MRI biomarker of tumour response in clinical trials. Nat Rev Clin Oncol. 2014
41. Jain RK. Normalization of tumor vasculature: an emerging concept in antiangiogenic therapy. Science. 2005; 307(5706):58–62. [PubMed: 15637262]
42. Hlatky L, Hahnfeldt P, Folkman J. Clinical application of antiangiogenic therapy: microvessel density, what it does and doesn't tell us. J Natl Cancer Inst. 2002; 94(12):883–893. [PubMed: 12072542]
43. Claesson-Welsh L, Welsh M. VEGFA and tumour angiogenesis. J Intern Med. 2013; 273(2):114–127. [PubMed: 23216836]
44. Munshi N, Jeay S, Li Y, Chen CR, France DS, Ashwell MA, Hill J, Moussa MM, Leggett DS, Li CJ. ARQ 197, a novel and selective inhibitor of the human c-Met receptor tyrosine kinase with antitumor activity. Mol Cancer Ther. 2010; 9(6):1544–1553. [PubMed: 20484018]

45. di Tomaso E, Snuderl M, Kamoun WS, Duda DG, Auluck PK, Fazlollahi L, Andronesi OC, Frosch MP, Wen PY, Plotkin SR, Hedley-Whyte ET, Sorensen AG, Batchelor TT, Jain RK. Glioblastoma recurrence after cediranib therapy in patients: lack of “rebound” revascularization as mode of escape. Cancer Res. 2011; 71(1):19–28. [PubMed: 21199795]

46. Shojaei F, Lee JH, Simmons BH, Wong A, Esparza CO, Plumlee PA, Feng J, Stewart AE, Hu-Lowe DD, Christensen JG. HGF/c-Met acts as an alternative angiogenic pathway in sunitinib-resistant tumors. Cancer Res. 2010; 70(24):10090–10100. [PubMed: 20952508]

47. Yakes FM, Chen J, Tan J, Yamaguchi K, Shi Y, Yu P, Qian F, Chu F, Bentzien F, Cancilla B, Orf J, You A, Laird AD, Engst S, Lee L, Lesch J, Chou YC, Joly AH. Cabozantinib (XL184), a novel MET and VEGFR2 inhibitor, simultaneously suppresses metastasis, angiogenesis, and tumor growth. Mol Cancer Ther. 2011; 10(12):2298–2308. [PubMed: 21926191]

48. Ebos JM, Kerbel RS. Antiangiogenic therapy: impact on invasion, disease progression, and metastasis. Nat Rev Clin Oncol. 2011; 8(4):210–221. [PubMed: 21364524]

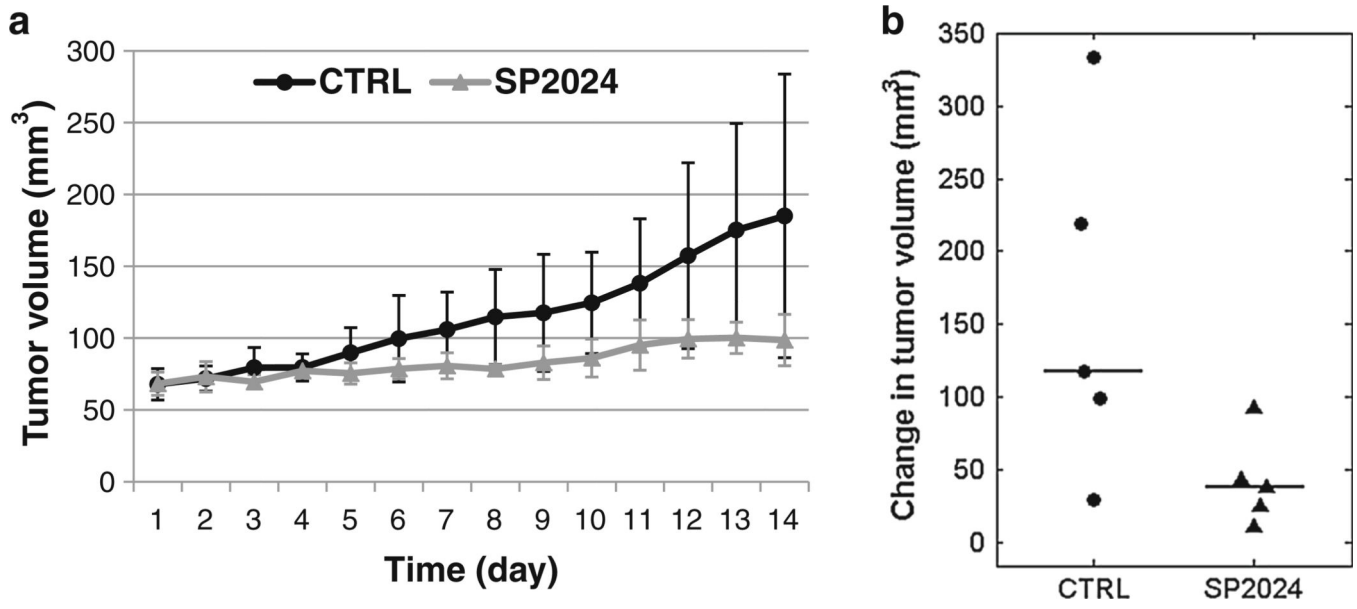

Fig. 1.

a Tumor growth curves showing the median tumor volumes of control (CTRL) and treated (SP2024) groups (n = 5 per group). *Error bars* indicate the median absolute deviation. **b** Dot plot of changes in tumor volume from day 0 to day 14 for individual tumors. *Horizontal lines* indicate the group medians

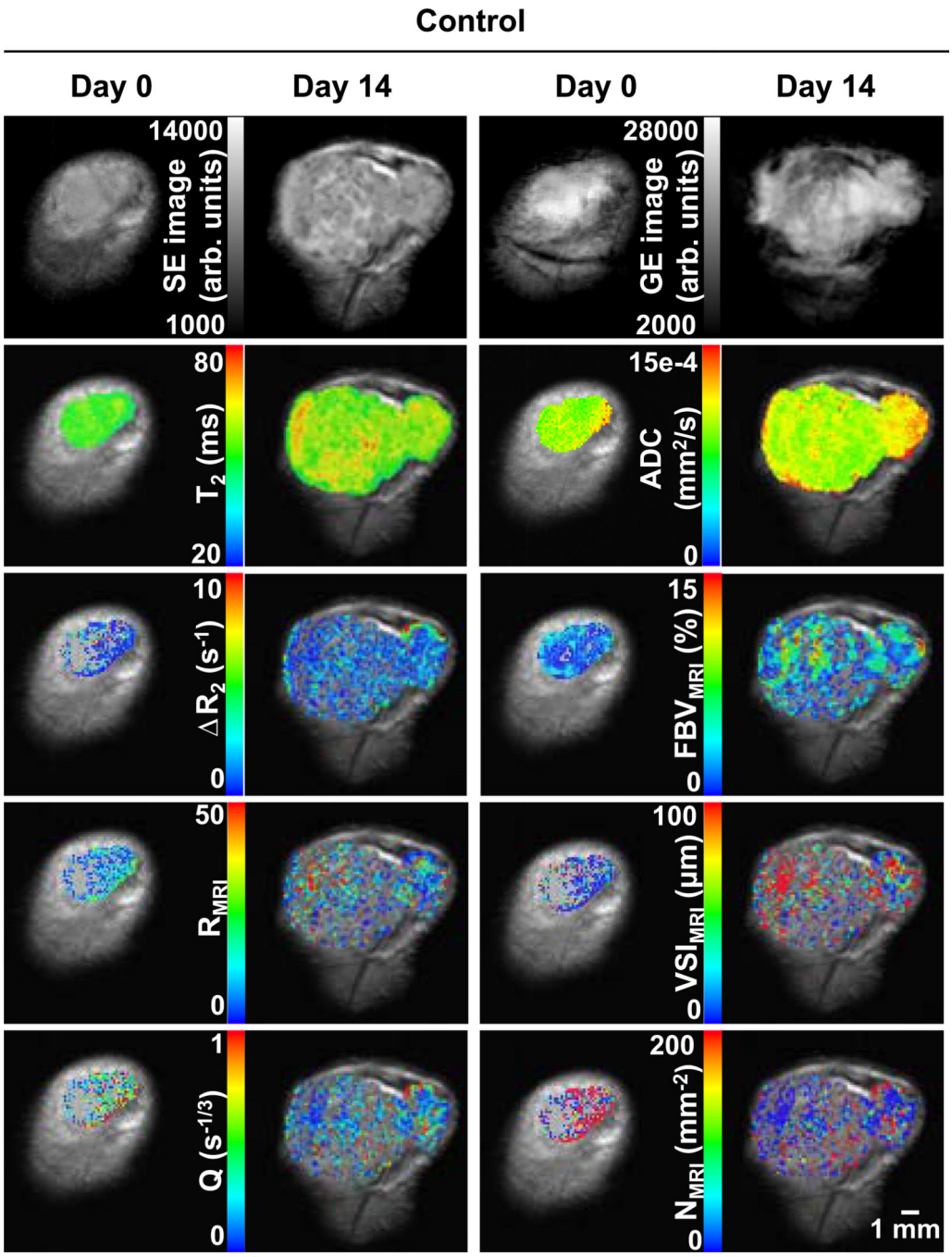

Fig. 2.

Raw images and parametric maps of a representative control tumor at day 0 and day 14. *Top row* raw spin echo (SE, TE = 40 ms) and gradient echo (GE, TE = 5 ms) images. *Second row* T_2 and ADC maps. *Third row* ΔR_2 (microvascular volume) and FBV (total blood volume) maps. *Fourth row R* and VSI maps (vessel radius). *Bottom row Q* and *N* maps (vessel density). Parametric maps are overlaid on their respective SE images. Overlay voxels with negative $\Delta R_2^{(*)}$ or that did not satisfy the *F*-stat criterion are not displayed

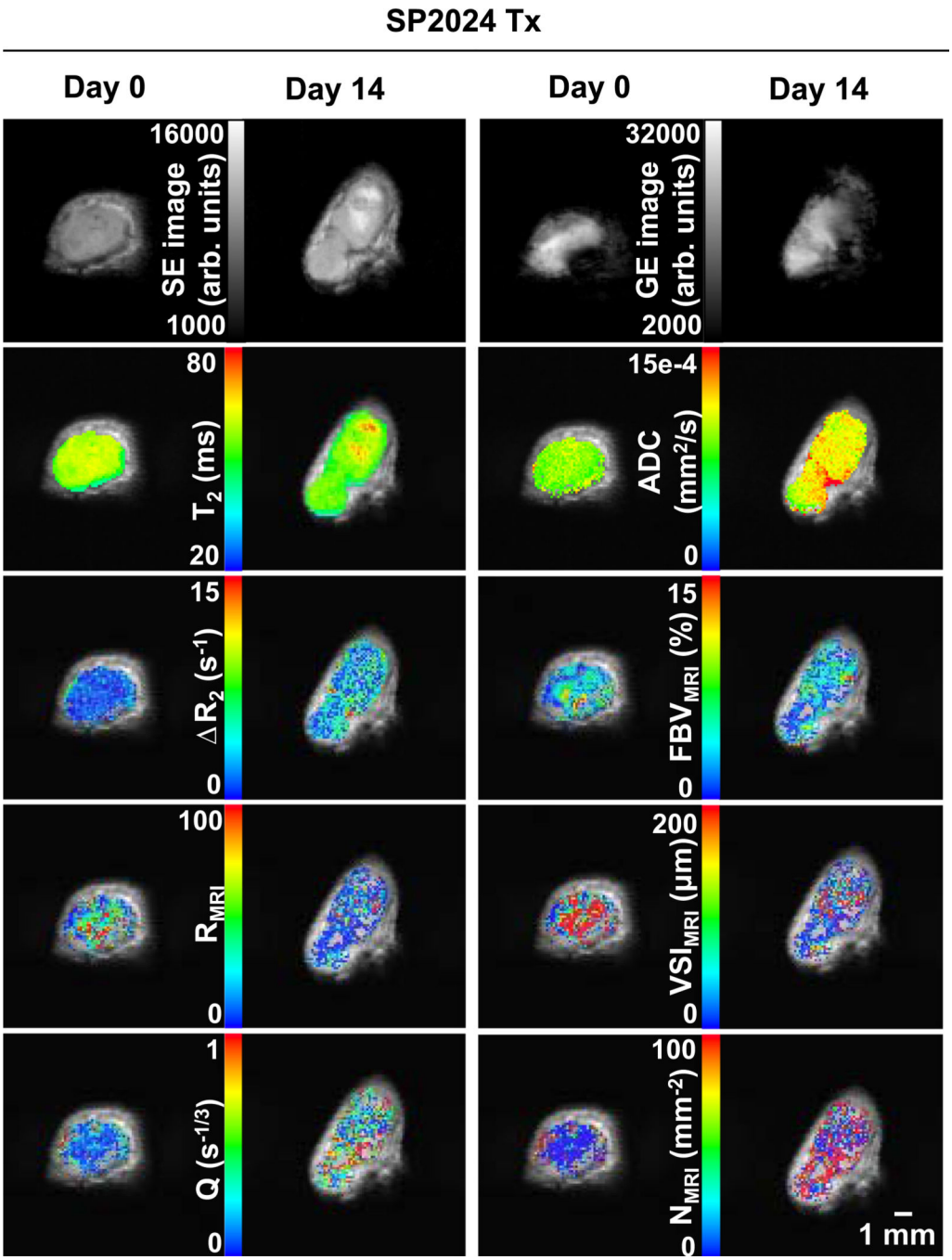

Fig. 3.

Raw images and parametric maps of a representative treated tumor at day 0 and day 14. *Top row* Raw SE (TE = 40 ms) and GE (TE = 5 ms) images. *Second row* T_2 and ADC maps. *Third row* ΔR_2 (microvascular volume) and FBV (total blood volume) maps. *Fourth row R* and VSI maps (vessel radius). *Bottom row Q* and *N* maps (vessel density). Parametric maps are overlaid on their respective SE images. Overlay voxels with negative $\Delta R_2^{(*)}$ or that did not satisfy the *F*-stat criterion are not displayed

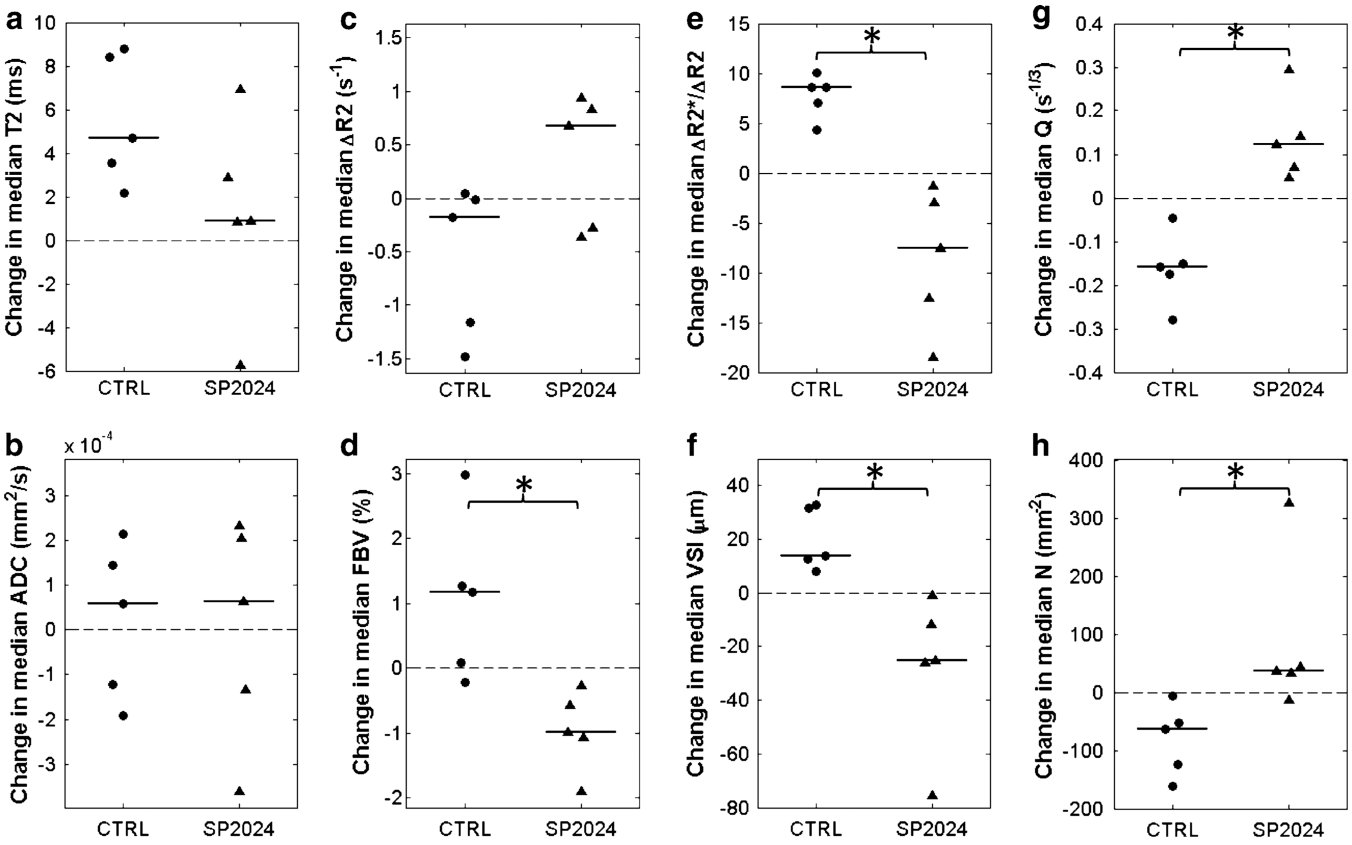

Fig. 4.

Dot plots of changes in tumor-wise median MRI biomarker values from day 0 to day 14 for control (CTRL) and treated (SP2024) tumors. *Horizontal lines* indicate group medians. There was no significant difference between control and treatment groups in the changes in T_2 (**a**) and ADC (**b**). With the exception of ΔR_2 (**c**), there was a significant difference in the changes in all of the vascular biomarkers (**d–h**). * $p < 0.05$, two-tailed Mann–Whitney *U* test

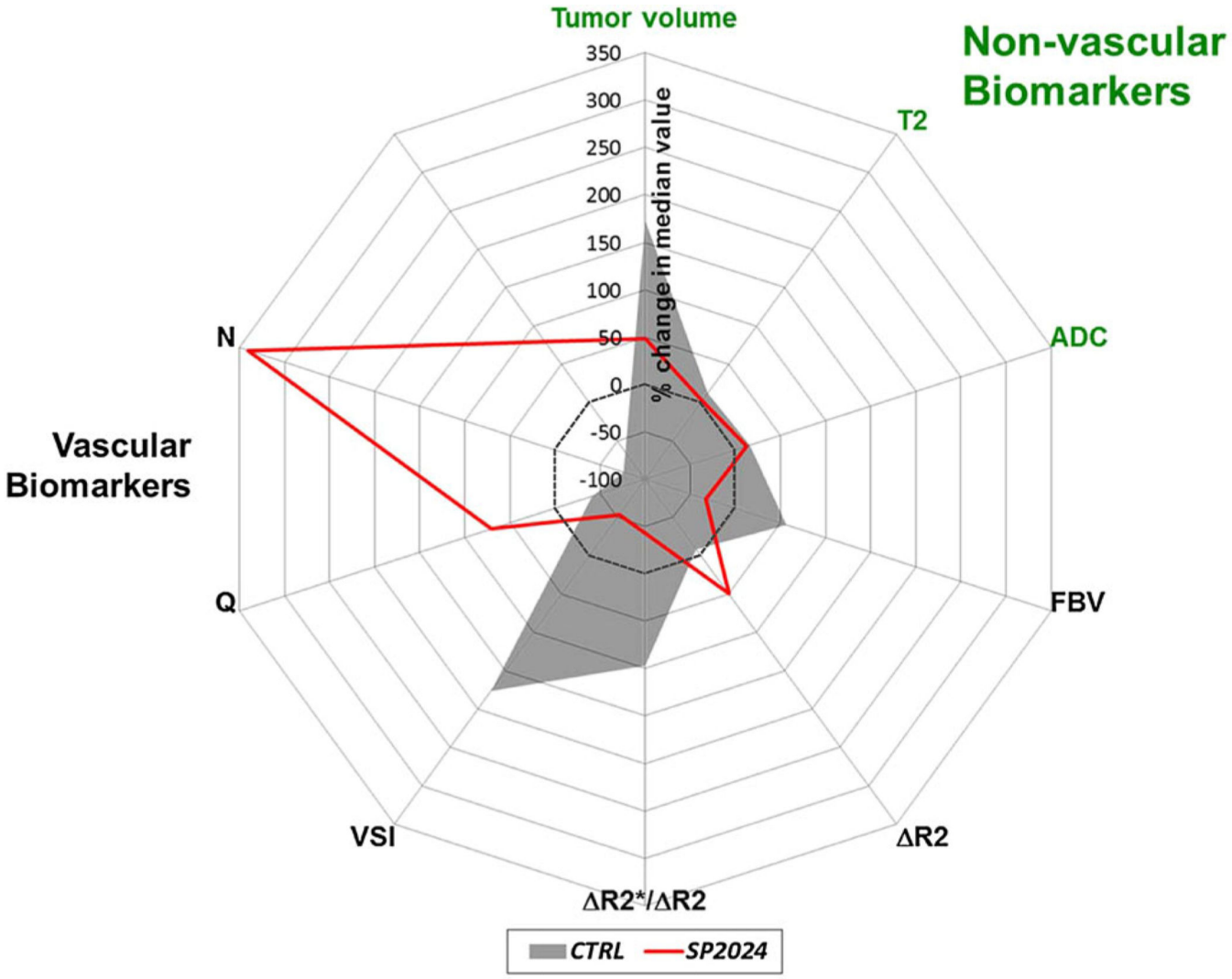

Fig. 5.

Radar plot of the percent changes in the median values of non-vascular and vascular MRI biomarkers for control (*gray fill*) and SP2024-treated (*red line*) groups. This clearly illustrates the sensitivity of vasculature-specific MRI biomarkers to the anti-angiogenic effects of SP2024 relative to the non-vascular or conventional MRI biomarkers

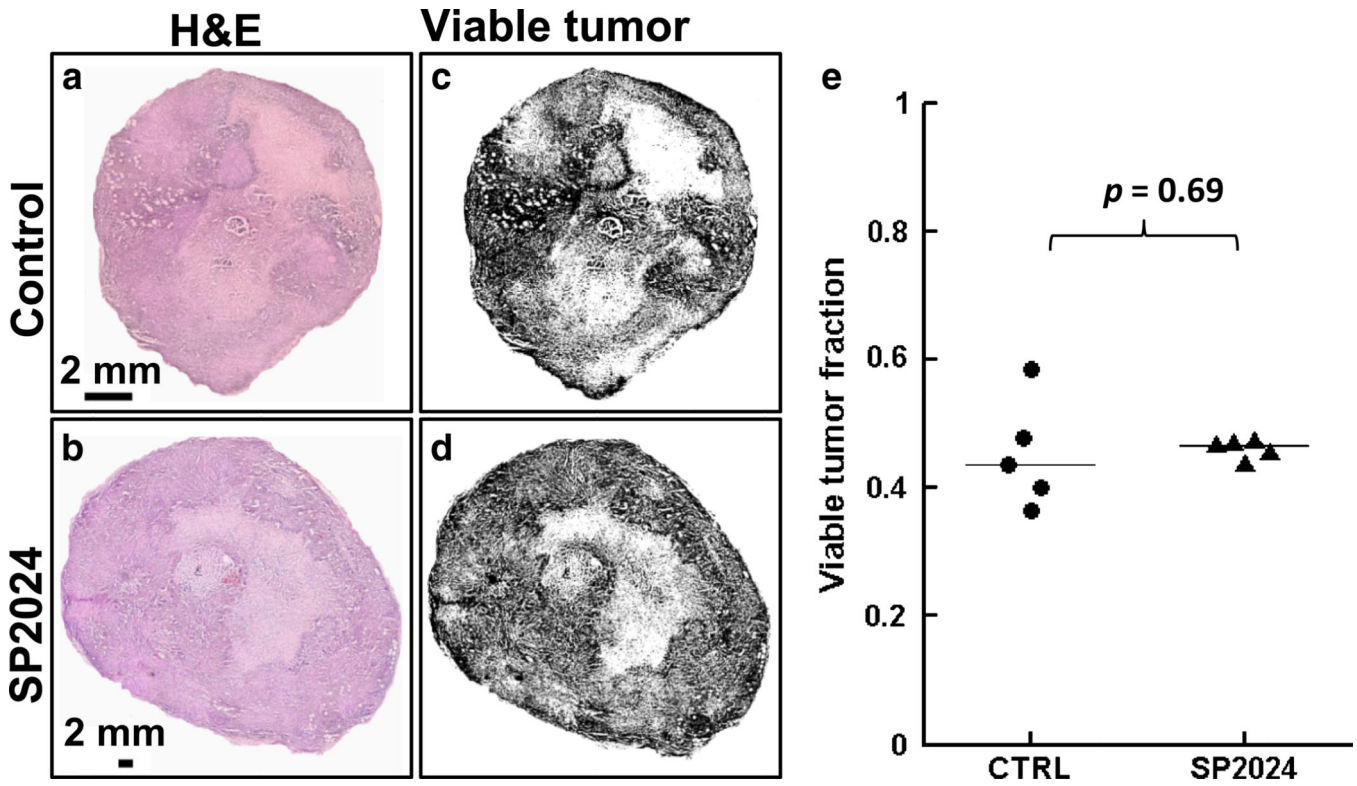

Fig. 6.

a, **b** Images of H&E sections from representative control and SP2024-treated tumors. **c**, **d** H&E images were binarized based on grayscale image intensity with black pixels representing viable tumor. **e** Dot plot of the viable tumor fractions of control and treated tumors, quantified from the binarized H&E images. *Horizontal lines* indicate the group medians

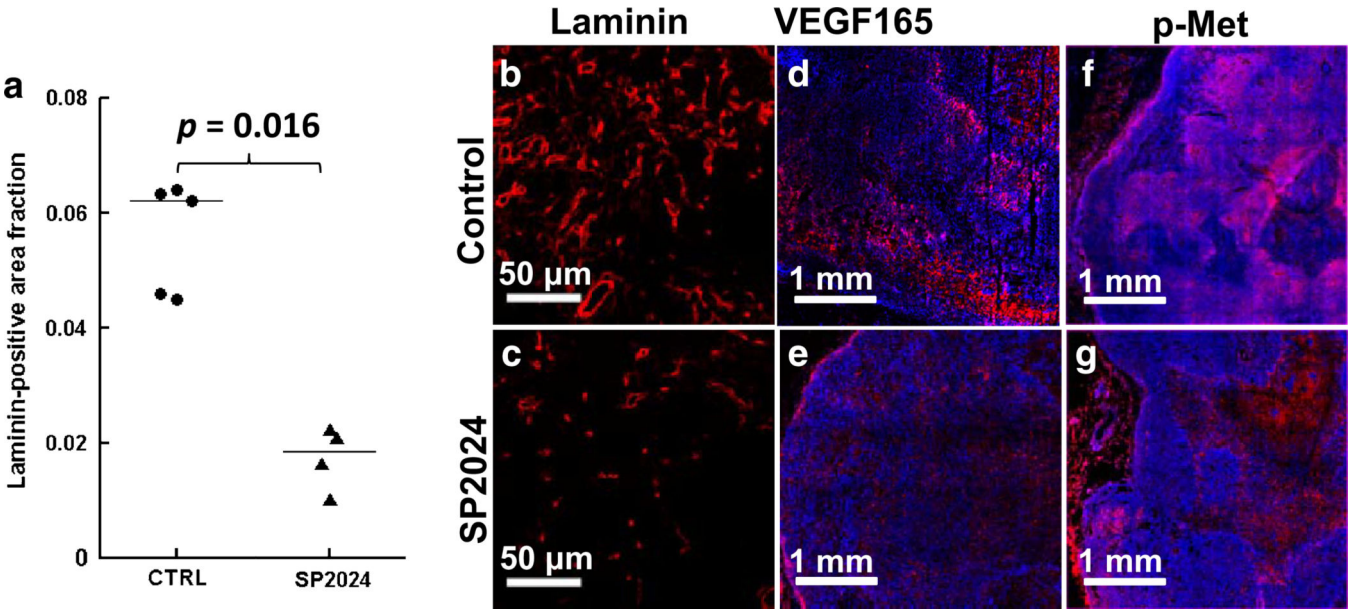

Fig. 7.

a Dot plot of tumor-wise average laminin-positive area fractions. *Horizontal lines* indicate the group medians. **b**, **c** 20× fluorescent images of representative laminin-stained sections from control and SP2024-treated tumors. **d**, **e** 10× fluorescent images of representative VEGF165-stained sections from control and treated tumors. **f**, **g** 10× fluorescent images of representative *p*-Met-stained sections from control and treated tumors

Table 1

Changes in median values of tumor parameters (median ± median absolute deviation)

	CTRL	SP2024	p^a
Tumor volume	117.2 ± 87.82 mm^3	38.41 ± 13.04 mm^3	0.06
	[172.9 ± 19.93 %]	[48.64 ± 15.20 %]	[0.06]
T_2	4.672 ± 2.496 ms^{-1}	0.888 ± 1.981 ms^{-1}	0.10
	[12.16 ± 5.676 %]	[2.473 ± 4.604 %]	[0.10]
ADC	5.830 ± 15.47 × 10^{-5} mm^2/s	6.369 ± 16.76 × 10^{-5} mm^2/s	1
	[16.00 ± 17.65 %]	[12.87 ± 47.38 %]	[0.84]
FBV	1.167 ± 1.081 %	−0.978 ± 0.416 %	<0.01
	[56.61 ± 54.22 %]	[−33.11 ± 11.54 %]	[<0.01]
ΔR_2	−0.182 ± 0.222 s^{-1}	0.673 ± 0.264 s^{-1}	0.22
	[−8.389 ± 10.16 %]	[49.94 ± 18.72 %]	[0.22]
$\Delta R_2^*/\Delta R_2$	8.598 ± 1.498	−7.556 ± 5.022	<0.01
	[96.91 ± 38.32 %]	[−42.43 ± 14.67 %]	[<0.01]
VSI	18.13 ± 7.133 μm	−25.75 ± 10.70 μm	<0.01
	[176.4 ± 110.4 %]	[−53.93 ± 5.384 %]	[<0.01]
Q	−0.159 ± 0.015 $s^{-1/3}$	0.122 ± 0.052 $s^{-1/3}$	<0.01
	[−49.09 ± 5.824 %]	[70.34 ± 42.59 %]	[<0.01]
N	−70.13 ± 50.17 mm^{-2}	37.37 ± 3.252 mm^{-2}	0.02
	[−75.88 ± 11.20 %]	[339.8 ± 176.1 %]	[<0.01]

Percent changes are reported in brackets

[a] Two-tailed Mann–Whitney *U* test between control and SP2024-treated tumors

Table 2

Mutual information between the percent changes in tumor-wise median parameter values and group membership (control or treated), used to quantify how well each parameter can distinguish between control and treated tumors

	Tumor volume	T_2	**ADC**	**FBV**	ΔR_2	$\Delta R_2^*/\Delta R_2$	**VSI**	Q	N
$I_{\max}$[a]	0.396	0.396	0.236	1	0.396	1	1	1	1
$I_{t=0}$[a]	0	0.108	0	0.610	0.125	1	1	1	0.610

[a] $I_{\max}$ is the maximum mutual information, and $I_{t=0}$ is the mutual information given only the direction of the change (i.e., an increase or decrease)